Hindawi
Journal of Chemistry
Volume 2017, Article ID 4361056, 11 pages
https://doi.org/10.1155/2017/4361056

Research Article

The Impact of Ce-Zr Addition on Nickel Dispersion and Catalytic Behavior for CO_2 Methanation of Ni/AC Catalyst at Low Temperature

Minh Cam Le, Khu Le Van, Thu Ha T. Nguyen, and Ngoc Ha Nguyen

Theoretical and Physical Chemistry Division, Faculty of Chemistry, Hanoi National University of Education, Hanoi 1000, Vietnam

Correspondence should be addressed to Minh Cam Le; camlm@hnue.edu.vn

Received 8 November 2016; Revised 31 January 2017; Accepted 26 February 2017; Published 13 March 2017

Academic Editor: Anton Kokalj

The CO_2 methanation was studied over 7 wt.% nickel supported on $Ce_{0.2}Zr_{0.8}O_2$/AC to evaluate the correlation of the structural properties with catalytic performance. The catalysts were investigated in more detail by means of X-ray diffraction (XRD), transmission electron microscopy (TEM), and scanning electron microscopy (SEM). A sample of 7 wt.% nickel loading supported on activated carbon (AC) was also prepared for comparison. The results demonstrated that the ceria-zirconia solid solution phase could disperse and stabilize the nickel species more effectively and resulted in stronger interaction with nickel than the parent activated carbon phase. Therefore, 7% Ni/$Ce_{0.2}Zr_{0.8}O_2$/AC catalyst exhibited higher activity for CO_2 reduction than 7% Ni//AC. It can attain 85% CO_2 conversion at 350°C and have a CH_4 selectivity of 100% at a pressure as low as 1 atm. The high activity of prepared catalysts is attributed to the good interaction between Ni and $Ce_{0.2}Zr_{0.8}O_2$ and the high CO_2 adsorption capacity of the activated carbon as well.

1. Introduction

Increasing emissions of carbon dioxide arising from the widespread production of energy from fossil fuels is a critical matter regarding greenhouse gases effect and, thus, global warming [1, 2]. Technologies including possible reduction or conversion of CO_2 give valuable advantages for protecting the environment by recycling CO_2 effectively based on the catalytic methanation [3–5]. Conversion of carbon oxides into methane

$$CO_2 + 4H_2 \rightleftarrows CH_4 + 2H_2O \quad (1)$$

is a exothermic reaction with $\Delta H^\circ = -165$ kJ/mol. The exothermic character of the methanation process causes problems with respect to an exact control of the reaction temperature, which can result in a further increased conversion of CO_2 [6]. Therefore, the development of catalysts for methanation of carbon dioxide is the key factor. Recently, results of Beuls et al. [7] and Jacquemin et al. [8] give evidences that at low temperature (<200°C) and atmospheric pressure the reaction takes place with very high selectivity.

Various metal-based catalysts have been studied for the CO_2 methanation reaction such as Fe [9], Ru [10], Co [11], Rh [12, 13], Pd [14, 15], Pt [16], and Ni [16, 17] supported on several oxides (SiO_2 [18], TiO_2 [19], Al_2O_3 [20, 21], ZrO_2 [22, 23], CeO_2 [24], and Ce-Zr mixed oxides [25, 26]) or porous materials (HZSM-5 [27], HUSY [28, 29]). Although the noble metals (Ru, Rh, and Pd) exhibit better activity, they are too expensive for a large-scale industrial application; therefore nonnoble metal-based catalysts are often preferred. Among group VIII metals, the nickel-based catalysts have covered the larger part of published works [30–35] due to their high catalytic activity, high selectivity for methane, and relatively low price. The main problems of Ni-based catalysts are the deactivation due to carbon deposition and poor stability at high temperature [29, 34]. Therefore, great efforts have been made to develop an effective promoted Ni-based catalyst which exhibits both high activity and high thermal stability in CO_2 methanation.

Firstly, adding catalyst promoters, Trovarelli et al. [36, 37], who compared the catalytic activity of several Rh-based catalysts using different types of supports, CeO_2, SiO_2, Ta_2O_2,

and Nb_2O_5, found that the catalytic activity and thermal stability of the catalyst could be improved by using CeO_2 or ZrO_2 as the support. Rynkowski et al. [38] reported that Ni (or Ru) supported on Al_2O_3 (or SiO_2) which is promoted with CeO_2 possessed an improved activity for CO_2 hydrogenation into methane. The CO_2 methanation reaction using Ni supported on Ce-Zr mixed oxides catalysts was for the first time investigated by Ocampo et al. [39–41]. They found that these catalysts exhibited excellent levels of activity, selectivity, and stability for CO_2 methanation. Liu et al. [34] found that CeO_2 promoted the dispersion of metal Ni on the support and prevented the nickel species from sintering leading to the high activity and good stability. In addition, the presence of oxygen vacancies on the support, such as CeO_2, will create the additional driving force for the CO_2 conversion to CO in reducing atmosphere. Results from [42] seem to indicate that $Ce_xZr_{1-x}O_2$ ($0.5 < x < 0.8$) solid solution has a superior performance in terms of overall reduction and total oxygen storage.

Secondly, choosing a porous support, Wei and Jinlong [43] had written an overview about methanation of carbon dioxide. The article focuses on recent developments in catalytic materials, novel reactors, and reaction mechanism for methanation of CO_2. The authors demonstrated that the different interactions that can be established between the metal and the support shall influence the catalytic properties of the active metal sites. Jwa et al. [33] who studied the hydrogenation of carbon oxides (CO and CO_2) into methane over Ni/β-zeolite catalysts have the same result. In order to increase catalytic activity of the methanation, it is necessary to enhance CO_2 supply at the surface of the catalyst. Some researchers have studied nickel supported on porous alumina [44] or MCM41 [45, 46] catalysts and their results showed that the porous structure of the supports improved the dispersion of the nickel species on their surfaces and prevented the nickel species from sintering. Recently, activated carbon has been investigated by various research groups because of its large surface area, surface functionalization, and low energy requirements for regeneration. Their results indicated that activated carbon (AC) is a promising adsorbent for CO_2, at ambient conditions [47–49]. Vargas et al. [47] studied carbon dioxide adsorption at 273 K on three series of activated carbon monoliths prepared by impregnation of African palm shells. Their results showed that the carbon monoliths obtained can adsorb as much CO_2 as 5.8 mmol CO_2 g^{-1} at 1 bar and 273 K. Wickramaratne et al. [48, 49] indicated that the activated carbon spheres exhibited very high CO_2 uptake of 8.9 and 4.55 mmol/g at 0°C and 25°C under atmospheric pressure, respectively. In the work of Li et al. [50] pine cone shell-based activated carbons were used to adsorb CO_2. The results indicated good CO_2 adsorption of performance of activated carbon with a high adsorption capacity of 7.63 mmol g^{-1} and 2.35 mmol g^{-1} at 0°C under 1 and 0.15 bar pressure, respectively. In our previous work [51], the activation of carbon dioxide (CO_2) by catalytic systems comprising a transition metal (Co, Cu, and Ni) on an activated carbon (AC) support was investigated using a combination of different theoretical calculation methods: Monte Carlo simulation, DFT and DFT-D, molecular dynamics (MD), and a climbing image nudged elastic band (CI-NEB) method. The results obtained indicate that CO_2 is easily adsorbed by Ni/AC. Usually, catalytic reaction properties can be affected by the catalyst composition and structure (e.g., specific surface area, pore size distribution, pore size, and structure). As is generally known, the support with high surface area will make the dispersion of active sites more easily and consequently a higher active surface area is generated. Highly dispersed supported nickel catalysts have been widely used in the hydrogenation of CO_2 to methane. Activated carbon, which is characterized by large specific surface areas (>1000 m^2 g^{-1}) and developed pore structures, has exhibited good catalytic properties, thus making it of great interest to researchers in the field of catalysis. The nickel supported on activated carbon used for CO_2 catalytic hydrogenation had not been reported to date; we believe that activated carbon is a good support in modifying the surface properties to promote the nickel catalyst activity for hydrogenation of CO_2.

In this article, the Ni/AC and Ni/$Ce_{0.2}Zr_{0.8}O_2$/AC catalysts with 7 wt.% nickel loadings were prepared by the incipient wetness impregnation. In these catalysts, nickel species are considered as active sites supported on Tra Bac activated carbon (AC) or on $Ce_{0.2}Zr_{0.8}O_2$/AC (mixed oxides $Ce_{0.2}Zr_{0.8}O_2$ deposited on AC). The catalysts and the supports were characterized by XRD, SEM, TEM, H2-TPR, and nitrogen adsorption-desorption. The activity and the CH_4 selectivity of the catalyst samples for the CO_2 methanation were also performed by a continuous flowing microreactor apparatus. $Ce_{0.2}Zr_{0.8}O_2$ mixed oxide was chosen because it promoted the dispersion of the nickel species on the supports and prevented the nickel species from sintering, leading to the high activity and the good stability. Activated carbon can act as a storage source of both H_2 and CO_2 and it helps in making the dispersion of nickel on the surface much easier. The highly dispersed nickel species are easily reduced and they are responsible for the high catalytic performance and for reducing the inactive carbon deposition. The goals of this study are to report the effects of CeO_2-ZrO_2 promoter and of the pore structure of activated carbon on the dispersion of nickel species, as well as the catalytic performances for CO_2 methanation. The possible reasons for the effect of $Ce_{0.2}Zr_{0.8}O_2$ promoter on the catalytic activity of the Ni/AC catalyst were given.

2. Experimental

2.1. Catalyst Preparation

2.1.1. Preparation of Ni Catalyst with Activated Carbon as the Support. The Ni/AC was prepared by incipient wetness impregnation method at a nickel loading of 7 wt%. Typically, 1.74 g nickel nitrate hexahydrate, $Ni(NO_3)_2{\cdot}6H_2O$ (99.0%, Merck), was dissolved in 30 mL distilled water. Then 5 g activated carbon support (coconut shell activated carbon was provided by Tra Bac factory, Vietnam) that was previously washed, crushed, and sieved to a size of 0.65–1 mm was added. The samples, subsequently, were dried in an oven at 60°C for 10 hours and continuously at 100°C for another

5 hours. Finally, the samples were calcined in N_2 environment at 400°C for 4 hours and then stored for further characterizations. The catalyst samples were denoted as 7 Ni/AC for weight percentage of 7% Ni.

2.1.2. Preparation of Ni Catalyst with $Ce_{0.2}Zr_{0.8}O_2$/AC as the Support. The mixed oxide $Ce_{0.2}Zr_{0.8}O_2$ was prepared using hydrothermal method as in the work of Pham et al. [52]. Typically, 1.6 mmol $Ce(NO_3)_3{\cdot}6H_2O$ (98.5%, Merck, Darmstadt, Germany) and 6.4 mmol $ZrOCl_2{\cdot}8H_2O$ (99.0%, Merck) were dissolved with 16 mmol urea-CH_4N_2O (98%, Merck) in 80 mL H_2O. The solution was then stirred until complete solubility. The obtained solution was poured into an autoclave, which was then maintained at 160°C for 24 h. The obtained light-yellow precipitate was washed with distilled water until constant pH and then dried at 80°C and finally calcined at 500°C for 4 hours.

$Ce_{0.2}Zr_{0.8}O_2$ was deposited on AC by suspension method: 5 g AC grains were immersed in 30 mL aqueous slurry of 20 wt% of $Ce_{0.2}Zr_{0.8}O_2$ powder, 20 vol% molten (70°C) Brij 56 (Sigma Aldrich, Steinheim, Germany), and 2.8 M HNO_3 and then dried and air blown. This coating and drying process was performed five times before calcination at 200°C for 4 h. The amount of $Ce_{0.2}Zr_{0.8}O_2$ on AC was determined by weighting the sample before (m_o) and after (m_t) the loading. The wt% loading was calculated as follows: wt% $= ((m_t - m_o)/m_o) \times 100$.

Nickel (the active phase, with the loading of 7 wt%) was deposited on the $Ce_{0.2}Zr_{0.8}O_2$/AC samples by wet impregnation. Suitable amount (1.74 g) of $Ni(NO_3)_2{\cdot}6H_2O$ (99.0 wt%, Merck) was dissolved in 30 mL distilled water; then the $Ce_{0.2}Zr_{0.8}O_2$/AC support was immersed in the prepared solution for 5 min. The wet pellets were dried until becoming completely dry. This procedure was repeated until all the solution ran out. Finally, the impregnated samples were heated at a heating rate of 3°C/min till 200°C and maintained at 200°C for 4 h. The catalyst sample was then symbolized as 7 Ni/CeZrAC.

2.2. Characterization of Catalysts. X-ray powder diffraction (XRD) patterns of the samples were obtained in a X-ray diffractometer (D8 Advance-Bruker) using Cu Kα radiation with a wavelength of 0.154 nm from 10° to 70° with a step size of 0.03°. The data were compared to reference data from JCPDS or ICDD. The particle size calculations were performed using the Scherrer equation.

Brunauer–Emmett–Teller (BET) specific surface areas, average pore diameter, and pore volume of the samples were determined by N_2 adsorption-desorption isotherm at 77 K using the BET (Brunauer–Emmett–Teller) method in a Micromeritics Tristar 3000 instrument. Before each measurement, the sample was degassed at 523 K for 4 hours.

The scanning electron microscopy (SEM) studies of the catalysts were performed on a scanning electron microscope (Hitachi S-4800) apparatus with an accelerating voltage of 10.0 kV. The samples were placed onto a metallic support and covered with a thin platinum film.

Transmission electron microscopy (TEM) studies were performed on a JEOL JEM-2000FX II instrument operated at 80.0 kV. All samples were suspended in ethanol by ultrasonication. The suspension was deposited on a copper grid with carbon film for TEM measurements.

Temperature-programmed reduction (TPR) measurements were carried out with a Micromeritics AutoChem 2920 instrument in a quartz U tube microreactor. Prior to the reduction the sample (app. 40 mg) was purged with Ar (50 mL min^{-1}) for 1 hour at 423 K to remove physically adsorbed water and then cooled down to room temperature. Afterwards, the sample is reduced in the flow of 10 vol% H_2/Ar (50 mL min^{-1}) at a heating rate of 10 K min^{-1} up to 973 K. The consumption of hydrogen was detected with a thermal conductivity detector (TCD) during the TPR procedure.

2.3. Evaluation of Catalysts. The gas phase hydrogenation of CO_2 to methane was carried out in a continuous-flow fixed-bed quartz reactor with an internal diameter of 1.5 mm under normal atmospheric pressure. A thermocouple was inserted into the catalyst bed to measure the reaction temperature. Typically for each run about 0.3 grams of catalyst pellets (similar size of 40–60 mesh) was loaded into a quartz reactor and reduced in situ under continuous flow of pure H_2 at the rate of 30 mL min^{-1}. The reduction temperature was programmed to increase from room temperature to 600°C and maintained at 600°C for 4 h. After reduction, the temperature was decreased to 100°C under the same hydrogenation flow and the catalyst was subsequently exposed to the feed gases $CO_2/H_2/He$ with a molar ratio of $CO_2 : H_2 : He = 1 : 4 : 5$ at a gas hourly space velocity (GHSV) of 4000 mL$\cdot g_{cat}^{-1} \cdot h^{-1}$ under atmospheric pressure. Catalytic activity was measured at 100, 200, 250, 300, 350, 400, and 450°C. At each temperature, after the stabilization of the catalytic system, three measures of CO, CO_2, and CH_4 were taken and an average value was calculated. The effluent gases were passed through a cold trap to condense water before being analyzed. The water level in the cold trap was low enough to prevent absorption of any gases. The analysis of evolved gases was conducted using an online GC (Trace-GC-RGA, Thermo Scientific) equipped with a thermal conductivity detector (TCD). The HayeSep Q capillary column ($8' \times 1/8''$ SS) is capable of separating CO_2 and C_1-C_2 paraffin and the Molecular Sieve 5A plot capillary column is capable of separating O_2, N_2, CH_4, and CO. During catalytic testing, carbon balances were calculated and were repeatedly between 97 and 99%.

Activity-selectivity data were obtained at steady-state conditions after 1 h of time on stream, at reaction temperatures. CO_2 conversion values (X_{CO_2}) were calculated by mass-balance method:

$$\text{Conversion of } CO_2 \ (\%) = \frac{\text{moles of } CO_2 \text{ reacted}}{\text{moles of } CO_2 \text{ supplied}} \times 100$$

$$\text{Selectivity for methane } (\%) = \frac{\text{moles of } CH_4 \text{ formed}}{\text{moles of } CO_2 \text{ reacted}} \times 100$$

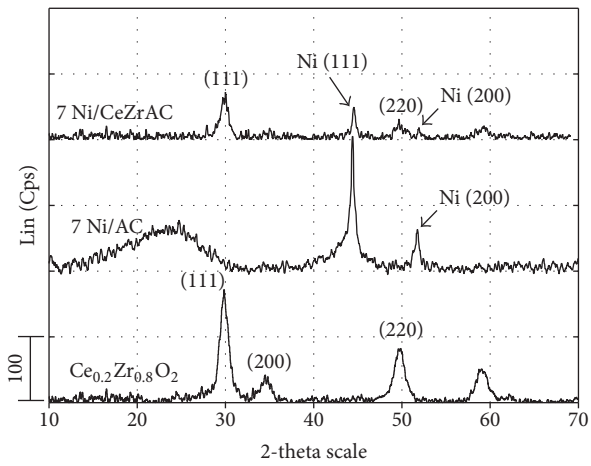

Figure 1: XRD patterns of $Ce_{0.2}Zr_{0.8}O_2$ and 7 Ni/AC and 7 Ni/CeZrAC reduced at 600°C for 4 hours.

$$\text{Selectivity for CO (\%)} = \frac{\text{moles of CO formed}}{\text{moles of } CO_2 \text{ reacted}} \times 100, \quad (2)$$

CH_4 formation rate is reported as number of molecules formed per unit time and per catalyst weight (mmol h^{-1} g_{cat}^{-1}).

Each data set was obtained with an accuracy of ±4%, from an average of two independent measurements.

3. Results and Discussion

3.1. XRD Characterization. The identification of the crystalline phases was carried out by XRD. The XRD patterns of 7 Ni/AC after reduction are presented in Figure 1. After reduction at 600°C in hydrogen atmosphere for 4 hours, all the reduced samples showed prominent peaks of metallic Ni at the $2\theta = 44.2°$ and 51° which are indexed to (111) and (200) diffractions planes, respectively. This matched the standard data for a cubic structure Ni (JCPDS 96-151-2527). No other peaks appear. It can be seen that the thermal treatment in H_2 at 600°C is sufficient for producing bulk Ni crystallites from nickel containing species.

The XRD patterns of mixed oxide $Ce_{0.2}Zr_{0.8}O_2$ and 7 Ni/CeZrAC after reduction were also displayed in Figure 1. The formation of $Ce_{0.2}Zr_{0.8}O_2$ on the AC was proved by XRD characterization. Phase transitions occurring in $Ce_xZr_{1-x}O_2$ depend on their composition. For pure ZrO_2 (Z) the diffraction peaks at $2\theta \approx 30.3°$, 34.6°, and 35.4° can be assigned to the tetragonal ZrO_2 structure (JCPDS 79-1769) and for pure CeO_2 (C) the diffraction peaks at $2\theta \approx 28.7°$ and 33.1° can be assigned to the cubic CeO_2 structure (JCPDS 65-5923). The work done by Hori et al. [53] showed that the tetragonal $Ce_xZr_{1-x}O_2$ phase appears with Ce < 50 mol% (C20Z), whereas above 50 mol%, a cubic $Ce_xZr_{1-x}O_2$ (C50Z and C80Z) phase is formed. With 80% Zr in our samples, the ceria peak originally at $2\theta \approx 28.6°$ is now at $2\theta \approx 30.0°$, which overlaps with a zirconia line at $2\theta \approx 30.1°$. In addition, we detected a doublet at $2\theta \approx 34.3°$ and 34.8° which is close to the tetragonal zirconia peaks at $2\theta \approx 34.6°$ and 35.4°. The peak at $2\theta \approx 34.9°$ is clearly a tetragonal zirconia line, shifted down 0.5° due to doping by small amounts of Ce. The peak with $2\theta \approx 34.3°$ is in a region where a cubic ceria-zirconia line (shifted up from $2\theta \approx 33.1°$, in pure CeO_2) overlaps with a tetragonal zirconia-ceria line (shifted down from $2\theta \approx 34.6°$, in pure ZrO_2). This shift is indicative of change in lattice parameter, and it is evident that CeO_2 and ZrO_2 form a solid solution. The powder possesses the diffraction peaks at 2θ = 30, 34.9, 49.7, and 58.5° related to the reflection planes (111), (200), (220), and (311) of $Ce_{0.2}Zr_{0.8}O_2$, respectively, showing the replacement of Zr atoms for Ce. Our measured lattice parameters are similar to those from reference materials [53]. Duwez and Odell [54] also obtained a tetragonal zirconia phase when high compositions of zirconia were used (around 80%), but for the sample containing 25% Zr they still obtained a cubic phase.

XRD pattern of 7 Ni/CeZrAC shows characteristic peaks of metallic Ni (2θ = 44.2° and 51°). There are also other diffraction peaks (at the 2θ values of 30, 49.7, and 59.6°) matching the standard data for a tetragonal mixed oxide $Ce_{0.2}Zr_{0.8}O_2$ (ICDD Card number 80-0785). The existence of ZrO_2 and CeO_2 or other species were not observed in XRD pattern of 7 Ni/CeZrAC. The presence of only tetragonal structure in the $Ce_{0.2}Zr_{0.8}O_2$ sample and in 7 Ni/CeZrAC as well indicates that Ce and Zr are highly homogeneously distributed. The approximate average crystallite sizes of mixed oxide $Ce_{0.2}Zr_{0.8}O_2$ in 7 Ni/CeZrAC sample and of pure $Ce_{0.2}Zr_{0.8}O_2$ were calculated by Scherrer's equation that indicates similar values. The approximate average crystallite sizes of Ni in catalyst samples were calculated from the (111) peak at 44,2° in the XRD patterns and Scherrer equation and are presented in Table 1. It can be seen that the Ni species dispersed well on the AC surface due to a high specific area of the support. However, the results show that the Ni particle size in 7 Ni/CeZrAC (17,39 nm) is smaller than that in 7 Ni/AC (21.82 nm) with pure AC as the support. This observation suggests that the dispersion of Ni species increases for the 7 Ni/CeZrAC catalyst due to the character of structural promoter of $Ce_xZr_yO_z$ mixed oxide. Since the XRD patterns exhibit identical 2θ angles, it can be said that the samples are completely reduced to metallic nickel without any detection of NiO_x phases, and the experimental procedure did not alter significantly the main crystalline phases of the samples.

3.2. N_2 Adsorption-Desorption Analysis (Table 2). BET surface areas, pore volume, and pore diameter of AC and of 7 Ni/AC reduced in H_2 at 600°C for 3 hours were listed in Table 2. It could be seen that activated carbon has a microporous structure and a developed specific surface area of 1159 m^2 g^{-1} with high microporous content (micro surface area is ~1139 m^2/g and microporous volume is ~0.5025 cm^3/g). The addition of nickel species resulted in slight decreases in surface areas and pore volume of the sample. This could be mainly attributed to a partial blockage of micropores by nickel species and the variation in mass

Table 1: Lattice parameters from XRD results and crystallite size of Ni (D) from Scherrer equation.

Catalyst samples		a	b	c	D (nm)
7 Ni/AC	Cubic	3.5350	3.5350	3.5350	21.82
7 Ni/CeZrAC:					
(i) Ni particle	Cubic	3.5240	3.5240	3.5240	17.39
(ii) $Ce_{0.2}Zr_{0.8}O_2$	Tetragonal	3.6325	3.6235	5.2288	8.78
Pure $Ce_{0.2}Zr_{0.8}O_2$	Tetragonal	3.6325	3.6325	5.2288	7.43

Table 2: Textural properties of AC, 7 Ni/AC, and 7 Ni/CeZrAC catalysts.

Catalyst samples	S_{BET} ($m^2 g^{-1}$)	S_{mic} ($m^2 g^{-1}$)	S_{ext} ($m^2 g^{-1}$)	V_{mic} ($cm^3 g^{-1}$)	V_{mes} ($cm^3 g^{-1}$)	$\overline{D}$ (nm)
AC	1159	1139	20	0.5025	0.0323	1.85
7 Ni/AC	923	908	15	0.3943	0.0302	1.84
7 Ni/CeZrAC	705	547	158	0.2404	0.3433	3.29

S_{BET}: BET surface area; S_{mic}, S_{ext}, and V_{mic}: micropore, external surface area, and micropore volume, calculated from t-plot method; V_{mes}: mesopore volume, calculated from BJH (Barrett-Joyner-Halenda) method; $\overline{D}$: Average pore width, calculated from $4V/S_{BET}$.

density of the catalyst. A decrease in the external surface area with the Ni loading was also observed, which could suggest that Ni species may deposit on the external surface of the support. However, for all samples, the active sites of the catalysts are accessible to the reactant molecules.

The textural properties of 7 Ni/CeZrAC which was reduced in H_2 at 600°C for 4 hours are also presented in Table 2. There was a strong decrease in surface area of AC when $Ce_{0.2}Zr_{0.8}O_2$ was introduced. It may be due to the deposition of $Ce_{0.2}Zr_{0.8}O_2$ on the AC surface, which blocked micropores leading to a strong decrease in micro surface area and a simultaneous increase in external surface areas and mesoporous volume. The wide pore diameter can provide favorable conditions for the reactant molecules to diffuse and transfer in the catalyst and it may be one reason for the better performance of the 7 Ni/CeZrAC in comparison to that of the 7 Ni/AC.

3.3. SEM and TEM Images. Morphologies of pure AC (Figure 2(a)) of mixed oxide $Ce_{0.2}Zr_{0.8}O_2$ (Figure 2(b)) and of catalyst sample 7 Ni/AC after reduction at 600°C for 4 hours (Figures 2(c) and 2(d)) were analyzed by SEM at 300 nm and 1.0 μm scales. For 7 Ni/AC it can be seen that the surface of the sample exhibits a high density block structure. SEM image showed well the existence of large cavities over the catalyst texture, likely originated from activated carbon surface (Figure 2(a)).

SEM images of 7 Ni/CeZrAC after reduction at 600°C for 4 hours were shown in Figures 2(e) and 2(f). A homogeneous distribution of spherical particles was obtained when $Ce_{0.2}Zr_{0.8}O_2$ was deposited on the AC surface. At higher magnification (Figure 2(f)), the catalyst showed morphology with spherical particles of about 50–60 nm. Further, the Ni particles could not be seen obviously on the support in SEM images, suggesting a better dispersion of Ni crystallite species that were doped into the ceria-zirconia solid solution.

TEM images of 7 Ni/AC and 7 Ni/CeZrAC after reduction at 600°C in H_2 atmosphere for 4 hours were shown in Figure 3 where black spots are Ni particles. It could be seen that Ni particles are well dispersed over $Ce_{0.2}Zr_{0.8}O_2$ layer which was deposited on the activated carbon support. The introduction of $Ce_{0.2}Zr_{0.8}O_2$ improved the formation of smaller particles. It can see easily that the particle's sizes from TEM results are in good agreement with XRD and BET analysis.

3.4. The Reducibility of the Catalysts. TPR-H_2 was carried out to study the reduction property of the catalysts. Figure 4 shows the TPR profiles of 7 Ni/CeZrAC and 7 Ni/AC. The TPR profiles of AC and $Ce_{0.2}Zr_{0.8}O_2$ are also presented for comparison. TPR profiles for studied samples display two distinct reduction bands in the temperature range of 160–350°C which can be attributed to the reduction of nickel species and another broad reduction band in the temperature range of 350–700°C corresponding to the reduction of the supports. In order to gain more insight into the TPR results, the profiles were deconvoluted into several Gaussian peaks. In the reduction profile of $Ce_{0.2}Zr_{0.8}O_2$ three peaks around 401–614°C are attributed to the reduction peaks of the surface oxygen and the bulk oxygen in $Ce_{0.2}Zr_{0.8}O_2$, respectively [26]. According to the literature [26], the existence of reduction peaks at temperatures below 600°C for the CeO_2 is assigned to the presence of surface and subsurface oxygen atoms, which are the main ones responsible for the improved CeO_2 oxygen storage capacity. It can be seen that these peaks are shifted to lower temperatures due to the presence of nickel indicating an existence of interaction between Ni and Ce. Similarly, two peaks around 638–693°C appearing in the profile of activated carbon are assigned for the reduction peaks of surface oxygen and bulk oxygen in AC and/or functional groups in AC. The addition of Ni species shifted these peaks to lower temperatures.

3.4.1. The Reduction of Ni Species in Ni-AC Catalysts. Regarding the reduction peaks of nickel species in 7 Ni/AC catalyst, it can be seen that three obvious reduction bands are observed: the first band (I) at the lowest-temperature with a maximum

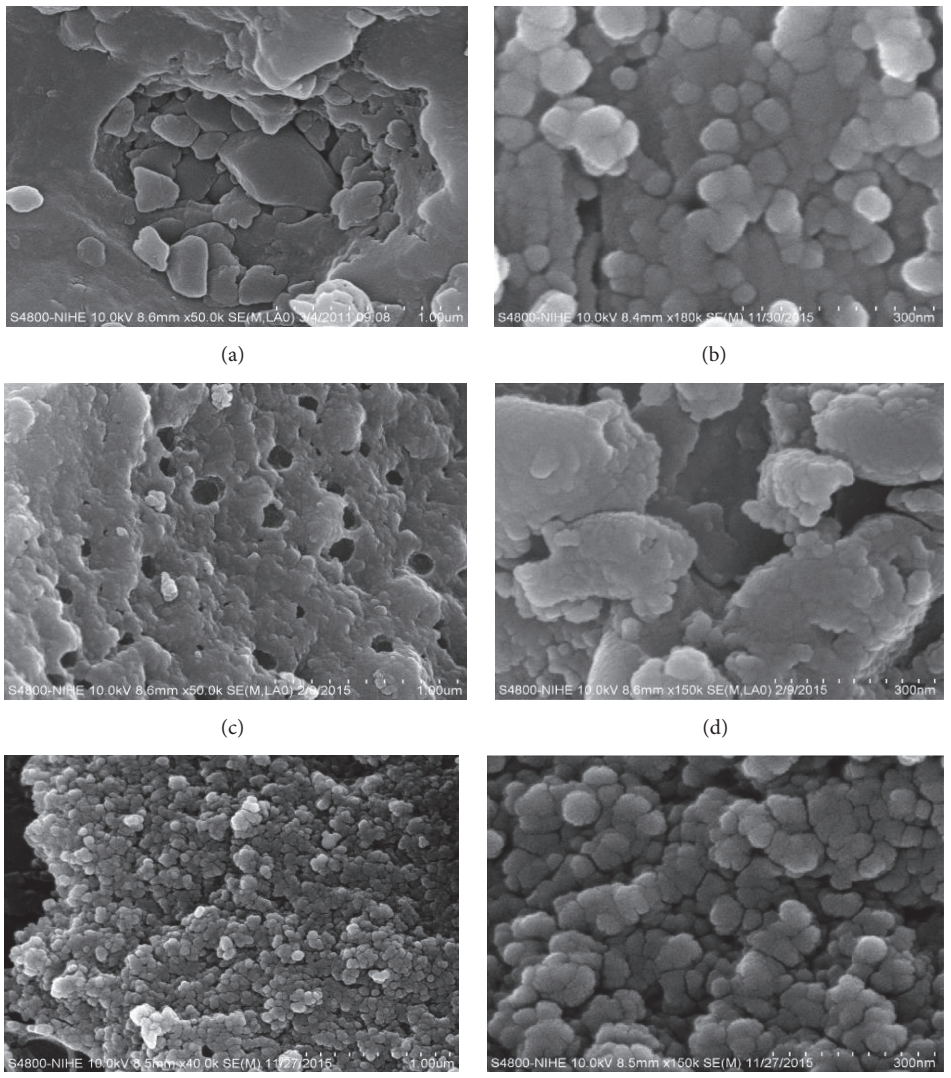

Figure 2: SEM images at 1.0 μm and 300 nm scales of AC (a), $Ce_{0.2}Zr_{0.8}O_2$ (b), 7 Ni/AC (c, d), and 7 Ni/CeZrAC (e, f).

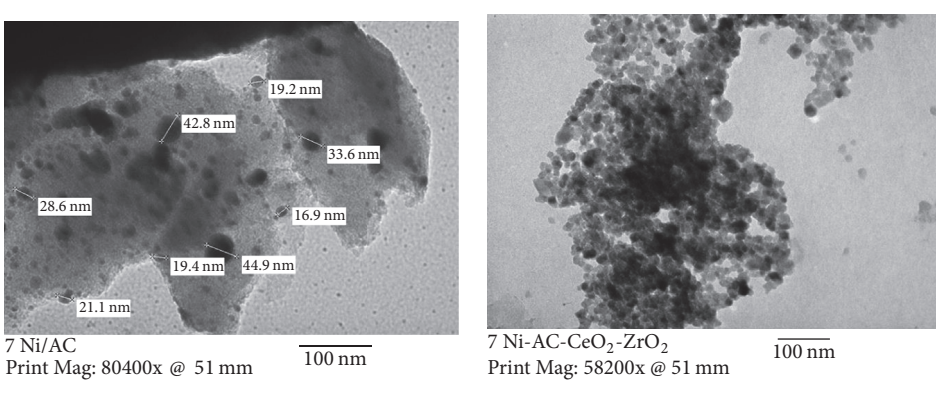

(a) 7 Ni/AC (b) 7 Ni/CeZrAC

Figure 3: TEM images of reduced catalyst samples.

Table 3: T_{max} and consumed H_2 for TPR patterns over studied catalysts.

Samples	T_{max} (°C)	H_2 consuming (mmol g^{-1})	Total H_2 consuming for first three peaks (mmol g^{-1})
7 wt% Ni/AC (7 Ni/AC)	231.3	0.33	2.62
	277.6	0.86	
	357.4	1.43	
	489.4	4.97	—
	579.8	1.88	
7 wt% Ni/$Ce_{0.2}Zr_{0.8}O_2$/AC (7 Ni/CeZrAC)	260.6	0.34	3.54
	290.7	1.66	
	345.1	1.54	
	504.7	2.72	—
	577.2	1.88	
$Ce_{0.2}Zr_{0.8}O_2$	428.1	0.09	0.64
	548.1	0.24	
	614.2	0.31	
AC	637.7	0.80	1.65
	693.0	0.85	

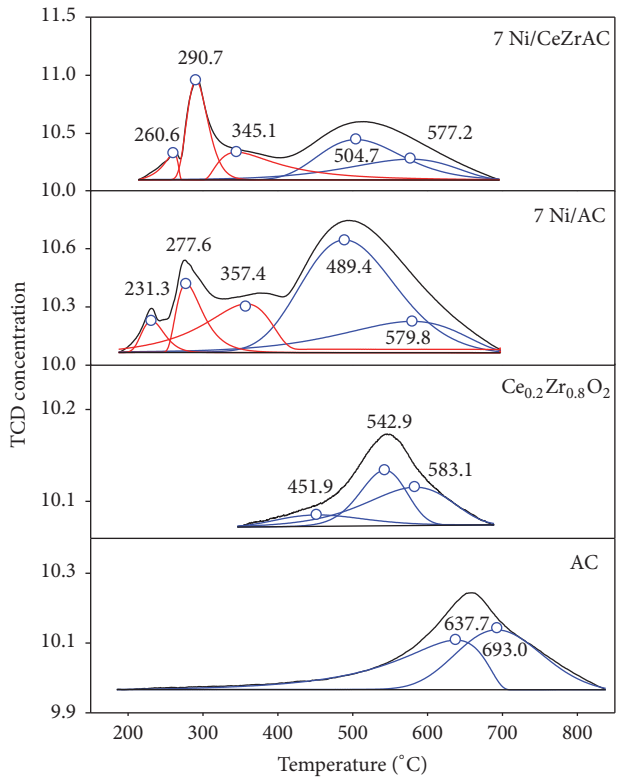

Figure 4: TPR-H_2 profiles of 7 Ni/AC and 7 Ni/CeZrAC.

around 228–231°C can be assigned to the well dispersed nickel species in the samples (may be assigned to the relatively free nickel species weakly interacting with support), which are easily reduced [29]. The low temperature band, the second band (II), shows a maximum at about 275–290°C, which may be due to the reduction of dispersed nickel species [55] and the third band (III) with a maximum around 343–357°C may be related to the reduction of bulk nickel species in intimate contact with the support [56]. The peak positions and their contribution are summarized in Table 3.

3.4.2. The Reduction of Ni Species in Ni/CeZrAC Catalyst. It can be seen that the curve of 7 Ni/CeZrAC is similar to that for 7 Ni/AC but the first three reduction peaks slightly shift toward the higher temperatures than in the 7 Ni/AC, which indicates a higher interaction between nickel species and the support ($Ce_{0.2}Zr_{0.8}O_2$/AC). Since $Ce_{0.2}Zr_{0.8}O_2$ and AC are not reducible at the temperature range of 160–350°C (as shown in their TPR-H_2 profiles), these first three peaks are attributed to the reduction of nickel species in the samples. Although the maximum reduction temperatures are slightly higher compared to that in 7 Ni/AC, the concentration of nickel species which can be easily reduced increases for 7 Ni/CeZrAC sample, indicating that the presence of Ce and Zr helps the dispersion of active sites and hence improves the reducibility of the sample. This attribution is in good agreement with that reported by Xu and Wang [57].

H_2 consumption of the supports and catalysts was calculated (Table 3). The obtained results show that the H_2 consumption of 7 Ni/CeZrAC catalyst (3.54 mmol g^{-1}) is higher than sum of 7 Ni/AC (2.62 mmol g^{-1}) and $Ce_{0.2}Zr_{0.8}O_2$ (0.64 mmol g^{-1}). It has been shown that the metal-support interaction between cerium-zirconium oxides and nickel oxides promotes the reducibility of samples [58]. This intimate metal-support interaction also promotes the dispersion of nickel oxide.

Based on TPR data, all samples were pretreated in H_2 at 600°C for 4 hours before measuring the catalytic activity in CO_2 hydrogenation reactions.

3.5. Catalytic Performance. Prior to the evaluation of the studied catalyst samples, the blank test in the absence of the

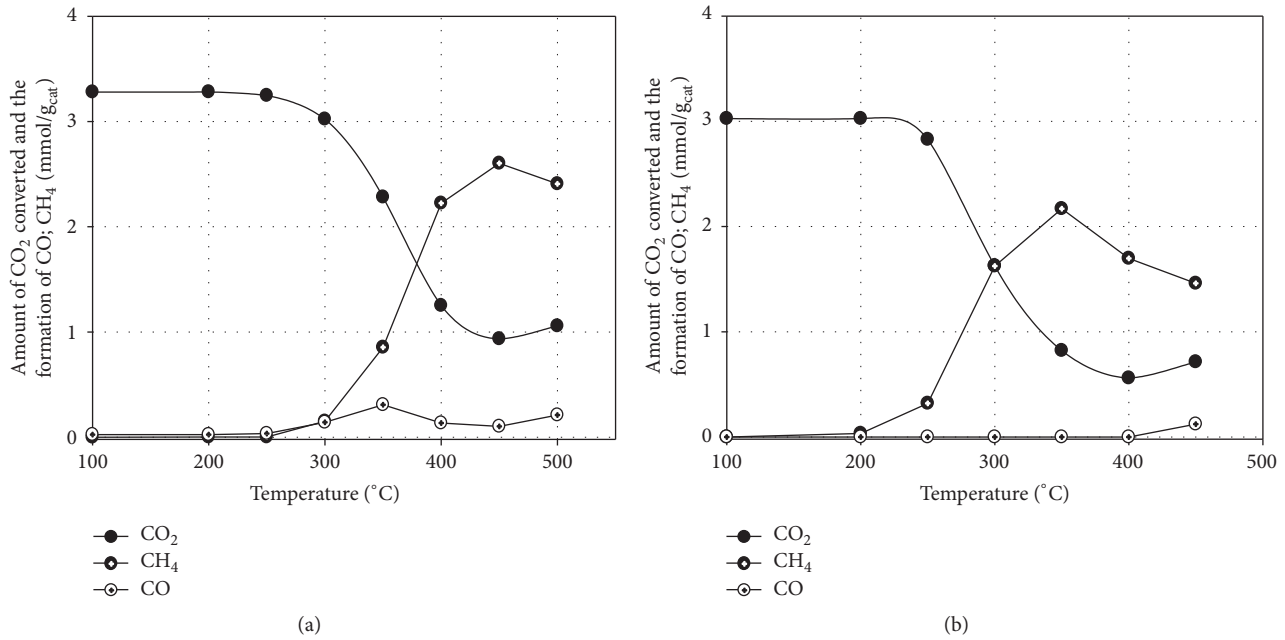

FIGURE 5: CO_2 conversion and CH_4 and CO selectivity versus temperature, at GHSV = 4000 mL/g_{cat}·h, 1 atm for 7 Ni/AC (a) and 7 Ni/CeZrAC (b).

catalyst sample was carried out in the range of 100–500°C and GHSV = 4000 mL h^{-1} g^{-1} (STP). The results showed that the blank reactor system was relative inert; only a negligible CO_2 conversion (<1%) could be detected under experimental conditions. Another two tests in the presence of pure AC and $Ce_{0.2}Zr_{0.8}O_2$/AC (without the presence of Ni species), respectively, were also performed under the same experimental conditions. It was found that not any CO_2 conversion and also CO or CH_4 were detected indicating that CH_4 and/or CO would be the products of CO_2 hydrogenation over studied Ni containing catalyst samples.

The catalytic activities of the samples were evaluated by analyzing the CO_2 conversion and CH_4 selectivity. In all experiments carried out only CH_4 and small amount of CO were detected at the outlet of the reactor; the carbon molar balances was about 97%.

Figures 5(a) and 5(b) present the CO_2 conversion and CH_4 and CO formation over 7 Ni/AC and 7 Ni/CeZrAC samples as a function of the reaction temperature.

3.5.1. The CO_2 Conversion. As seen in Figure 5 for both two samples, the amounts of CO_2 in the gas mixture decreased as temperature increased. The temperature at which the amount of CO_2 started going down was 200°C over 7 Ni/AC and 170°C over 7 Ni/CeZrAC. These phenomena indicated the conversion of CO_2 occurred and the conversion gradually increases with the temperature up to 450°C (over 7 Ni/AC) and 400°C (over 7 Ni/CeZrAC), but as further rise in temperature, the CO_2 conversion starts going down.

3.5.2. The CH_4 and CO Formation. There were two temperature ranges for product selectivity. At low temperature range of 200°C to 400°C over 7 Ni/AC and 170°C to 350°C over 7 Ni/CeZrAC, the formation of CH_4 was dominant; no alcohols or other hydrocarbons could be expected to be formed. CO formation was accompanied with CH_4 but very slightly. A further increase in the temperature (up to 500°C) will result in the stable increase in CO formation with the decrease of CO_2 conversion and the decrease of selectivity to methane formation as well. These phenomena are related to the thermodynamic nature of the CO_2 hydrogenation reaction because CO formation can occur mostly by the reversed water gas shift reaction (RWGS) and a small contribution depending on temperature from steam reforming (SR) of methane.

These observations are in good agreement with the work done by Graça et al. [29] and by Janke et al. [10].

3.6. The Effects of the Mixed Oxide $Ce_{0.2}Zr_{0.8}O_2$ Addition. A comparison in CO_2 conversion over 7 Ni/AC and 7 Ni/CeZrAC was made and shown Figure 6. It can be seen that the addition of solid solution $Ce_{0.2}Zr_{0.8}O_2$ is responsible for improvement of both CO_2 conversion and CH_4 selectivity: the conversion of CO_2 started at a lower temperature (170°C) compared to that of 7 Ni/AC sample (Figure 6), and it reached the maximum conversion value even at only 350°C. In the temperature range of 150–350°C no CO was detected at the outlet indicating a 100% for CH_4 selectivity (Figure 5(b)). This positive effect which shows the improvement of catalyst performance resulted from Ce-Zr well incorporation with Ni and AC surface.

It has been claimed in the literature that (Ce-Zr) species can activate CO_2 molecules and reduce them into CO due to the great mobility of the oxygen atoms. These CO species can be subsequently hydrogenated into methane. In the work

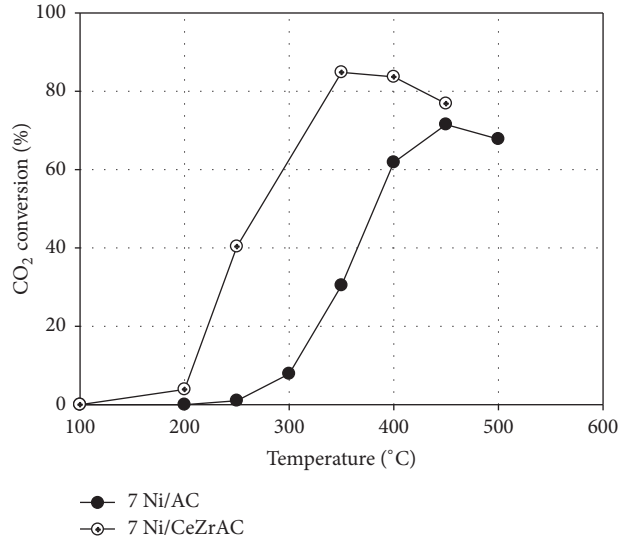

Figure 6: The comparison in CO_2 conversion between two Ni/AC samples with and without $Ce_{0.2}Zr_{0.8}O_2$: 7 Ni/AC and 7 Ni/CeZrAC.

done by Sharma et al. [13] Ru-doped ceria, $Ce_{0.95}Ru_{0.05}O_2$, prepared by a combustion method showed higher catalytic activity for CO_2 methanation than 5 wt% Ru/CeO_2 and the conversion of CO_2 and selectivity of CH_4 were 55% and 99%, respectively. By feeding 13% CO_2, 54% H_2, and 33% Ar at 450°C and GHSV = ca. 10,000 h^{-1}, Wang et al. [25] indicated that $Ni/Ce_{0.5}Zr_{0.5}O_2$ catalysts prepared by impregnation method possessed the highest activity for CO_2 hydrogenation. It can attain 73% conversion at 300°C and have a CH_4 selectivity of 100%.

The $Ni/Ce_{0.2}Zr_{0.8}O_2$/AC catalyst prepared in the present work had an excellent activity for CO_2 methanation at lower temperatures and a high CH_4 selectivity of 100%. TPR-H_2 characterization indicated the intimate interaction between the metal and the support that could promote the reduction of $Ce_{0.2}Zr_{0.8}O_2$, while the strong interaction inhibits the reduction of Ni species. Swalus et al. [21] indicated that nickel supported on AC is able to activate high amount of hydrogen, while Rynkowski et al. [38] reported that $Ce_{0.2}Zr_{0.8}O_2$ could supply the surface oxygen sites for CO_2 adsorption. Also, our previous theoretical study [51] showed that nickel plays an important role in the dissociative adsorption of CO_2. In that work the adsorption of carbon dioxide on AC was studied in two steps: (i) GCMC (grand canonical ensemble Monte Carlo) simulation to determine the most favorable adsorption positions; (ii) these configurations optimized using the DFT and DFT-D2 methods. Results obtained from the GCMC simulation showed that the CO_2 molecule is most favorably physically adsorbed on the surface of AC. The preferred configurations were then optimized to determine the adsorption energy of CO_2 on AC (Eads). The results obtained using the DFT and DFT-D2 methods were −27.3 kJ/mol and −46.9 kJ/mol, respectively, which indicate that CO_2 is easily adsorbed on the AC. When Ni was doped on the AC surface, the CO_2 molecule was chemically adsorbed and the C-O bond is strongly activated after the adsorption of CO_2. The adsorption process of CO_2 did not involve a transition state. Our calculated results showed that CO_2 adsorption and dissociation are the first steps in the mechanism of CO_2. Jacquemin et al. [8] had the same statement that the first step of the mechanism in the methanation reaction could be the chemisorption of CO_2 on the catalyst and followed by the dissociation of CO_2 into CO and O adsorbed on the surface. From obtained results we suggested that using AC as a carrier may lead to a significant increase of the partial pressure of CO_2 on the surface of the catalyst. In other words, the conversion of CO_2 with high efficiency can be carried out at unusually low pressures due to the increased CO_2 partial pressure on the AC surface. Our results give an evidence that at low temperature and at atmospheric pressure, it is possible to obtain methane from hydrogenation of CO_2 when using an adequate catalyst. The work done by Beuls et al. [7] shows the same conclusion, but the catalyst used was $Rh/\gamma\text{-}Al_2O_3$.

4. Conclusion

The present work investigated the correlation between structural properties and catalytic performance of 7 Ni/AC and 7 $Ni/Ce_{0.2}Zr_{0.8}O_2$/AC catalysts for CO_2 methanation reaction. The characterization of the samples by XRD,SEM, TEM, BET, and H_2-TPR techniques indicated that the dispersion of Ni species on the AC or $Ce_{0.2}Zr_{0.8}O_2$/AC was influenced by the structure of the supports and $Ce_{0.2}Zr_{0.8}O_2$/AC could stabilize the nickel species more effectively than AC. The characterized results suggested that Ni species interacted with $Ce_{0.2}Zr_{0.8}O_2$/AC more strongly than that with AC, and compared with the AC support the $Ce_{0.2}Zr_{0.8}O_2$/AC support had greater ability to facilitate the reduction of Ni species. The "synergistic effect" between the metal active sites (Ni), the promoter ($Ce_{0.2}Zr_{0.8}O_2$), and the support (AC) could promote the activation of adsorbed CO_2; therefore 7 $Ni/Ce_{0.2}Zr_{0.8}O_2$/AC showed the higher activity toward hydrogenation of CO_2 to methane than 7 Ni/AC. Our results suggest that the use of dissociative chemisorption of CO_2 could probably allow decreasing reaction temperature and the methanation of CO_2 at low temperature could be a solution for the control of increasing emission of CO_2.

Conflicts of Interest

The authors declare that there are no conflicts of interest regarding the publication of this paper.

Acknowledgments

Financial support from Ministry of Training and Education, Vietnam, under Project no. B2013-17-38, is gratefully acknowledged.

References

[1] M. Burkhardt and G. Busch, "Methanation of hydrogen and carbon dioxide," *Applied Energy*, vol. 111, pp. 74–79, 2013.

[2] F. T. Zangeneh, S. Sahebdelfar, and M. T. Ravanchi, "Conversion of carbon dioxide to valuable petrochemicals: an approach

to clean development mechanism," *Journal of Natural Gas Chemistry*, vol. 20, no. 3, pp. 219–231, 2011.

[3] R. Ladera, F. J. Pérez-Alonso, J. M. González-Carballo, M. Ojeda, S. Rojas, and J. L. Fierro, "Catalytic valorization of CO_2 *via* methanol synthesis with Ga-promoted Cu–ZnO–ZrO_2 catalysts," *Applied Catalysis B: Environmental*, vol. 142-143, pp. 241–248, 2013.

[4] G. Bonura, M. Cordaro, C. Cannilla, F. Arena, and F. Frusteri, "The changing nature of the active site of Cu-Zn-Zr catalysts for the CO_2 hydrogenation reaction to methanol," *Applied Catalysis B: Environmental*, vol. 152-153, pp. 152–161, 2014.

[5] P. Sabatier and J. B. Senderens, "Hydrogénation directe des oxydes du carbone eu présence de divers métaux divisés," *Comptes Rendus de l'Académie des Sciences Paris*, vol. 134, p. 689, 1902.

[6] S. Rahmani, M. Rezaei, and F. Meshkani, "Preparation of highly active nickel catalysts supported on mesoporous nanocrystalline γ-Al_2O_3 for CO_2 methanation," *Journal of Industrial and Engineering Chemistry*, vol. 20, no. 4, pp. 1346–1352, 2014.

[7] A. Beuls, C. Swalus, M. Jacquemin, G. Heyen, A. Karelovic, and P. Ruiz, "Methanation of CO_2: further insight into the mechanism over Rh/γ-Al_2O_3 catalyst," *Applied Catalysis B: Environmental*, vol. 113-114, pp. 2–10, 2012.

[8] M. Jacquemin, A. Beuls, and P. Ruiz, "Catalytic production of methane from CO_2 and H_2 at low temperature: insight on the reaction mechanism," *Catalysis Today*, vol. 157, no. 1–4, pp. 462–466, 2010.

[9] M. Schoder, U. Armbruster, and A. Martin, "Heterogeneously catalyzed hydrogenation of carbon dioxide to methane at increased reaction pressures," *Chemie-Ingenieur-Technik*, vol. 85, no. 3, pp. 344–352, 2013.

[10] C. Janke, M. S. Duyar, M. Hoskins, and R. Farrauto, "Catalytic and adsorption studies for the hydrogenation of CO2 to methane," *Applied Catalysis B: Environmental*, vol. 152-153, no. 1, pp. 184–191, 2014.

[11] G. Zhou, T. Wu, H. Xie, and X. Zheng, "Effects of structure on the carbon dioxide methanation performance of Co-based catalysts," *International Journal of Hydrogen Energy*, vol. 38, no. 24, pp. 10012–10018, 2013.

[12] A. Karelovic and P. Ruiz, "Mechanistic study of low temperature CO_2 methanation over Rh/TiO_2 catalysts," *Journal of Catalysis*, vol. 301, pp. 141–153, 2013.

[13] S. Sharma, Z. Hu, P. Zhang, E. W. McFarland, and H. Metiu, "CO2 methanation on Ru-doped ceria," *Journal of Catalysis*, vol. 278, no. 2, pp. 297–309, 2011.

[14] J.-N. Park and E. W. McFarland, "A highly dispersed Pd-Mg/SiO_2 catalyst active for methanation of CO_2," *Journal of Catalysis*, vol. 266, no. 1, pp. 92–97, 2009.

[15] H. Y. Kim, H. M. Lee, and J. Park, "Bifunctional mechanism of CO_2 methanation on Pd-MgO/SiO_2 catalyst: independent roles of MgO and Pd on CO_2 methanation," *The Journal of Physical Chemistry C*, vol. 114, no. 15, pp. 7128–7131, 2010.

[16] D. C. D. Da Silva, S. Letichevsky, L. E. P. Borges, and L. G. Appel, "The Ni/ZrO_2 catalyst and the methanation of CO and CO_2," *International Journal of Hydrogen Energy*, vol. 37, no. 11, pp. 8923–8928, 2012.

[17] M. A. A. Aziz, A. A. Jalil, S. Triwahyono, R. R. Mukti, Y. H. Taufiq-Yap, and M. R. Sazegar, "Highly active Ni-promoted mesostructured silica nanoparticles for CO2 methanation," *Applied Catalysis B: Environmental*, vol. 147, pp. 359–368, 2014.

[18] R. Razzaq, H. Zhu, L. Jiang, U. Muhammad, C. Li, and S. Zhang, "Catalytic methanation of CO and CO2 in coke oven gas over Ni-Co/ZrO2-CeO2," *Industrial and Engineering Chemistry Research*, vol. 52, no. 6, pp. 2247–2256, 2013.

[19] C. Deleitenburg and A. Trovarelli, "Metal-support interactions in Rh/CeO2, Rh/TiO2, and Rh/Nb2O5 catalysts as inferred from CO2 methanation activity," *Journal of Catalysis*, vol. 156, no. 1, pp. 171–174, 1995.

[20] K. Zhao, Z. Li, and L. Bian, "CO2 methanation and co-methanation of CO and CO2 over Mn-promoted Ni/Al2O3 catalysts," *Frontiers of Chemical Science and Engineering*, vol. 10, no. 2, pp. 273–280, 2016.

[21] C. Swalus, M. Jacquemin, C. Poleunis, P. Bertrand, and P. Ruiz, "CO2 methanation on Rh/γ-Al2O3 catalyst at low temperature: "in situ" supply of hydrogen by Ni/activated carbon catalyst," *Applied Catalysis B: Environmental*, vol. 125, pp. 41–50, 2012.

[22] M. Cai, J. Wen, W. Chu, X. Cheng, and Z. Li, "Methanation of carbon dioxide on Ni/ZrO_2-Al_2O_3 catalysts: effects of ZrO_2 promoter and preparation method of novel ZrO_2-Al_2O_3 carrier," *Journal of Natural Gas Chemistry*, vol. 20, no. 3, pp. 318–324, 2011.

[23] J. Ren, X. Qin, J.-Z. Yang et al., "Methanation of carbon dioxide over Ni-M/ZrO_2 (M = Fe, Co, Cu) catalysts: effect of addition of a second metal," *Fuel Processing Technology*, vol. 137, pp. 204–211, 2015.

[24] L. Liu, Z. Yao, B. Liu, and L. Dong, "Correlation of structural characteristics with catalytic performance of CuO/CexZr1−xO2 catalysts for NO reduction by CO," *Journal of Catalysis*, vol. 275, no. 1, pp. 45–60, 2010.

[25] S. Wang, Q. Pan, J. Peng, T. Sun, D. Gao, and S. Wang, "CO2 methanation on Ni/Ce0.5Zr0.5O2 catalysts for the production of synthetic natural gas," *Fuel Processing Technology*, vol. 123, pp. 166–171, 2014.

[26] F. Ocampo, B. Louis, A. Kiennemann, and A. C. Roger, "CO_2 methanation over Ni-Ceria-Zirconia catalysts: effect of preparation and operating conditions," *IOP Conference Series: Materials Science and Engineering*, vol. 19, no. 1, Article ID 012007, 2011.

[27] S. Scirè, C. Crisafulli, R. Maggiore, S. Minicò, and S. Galvagno, "Influence of the support on CO2 methanation over Ru catalysts: an FT-IR study," *Catalysis Letters*, vol. 51, no. 3-4, pp. 41–45, 1998.

[28] S. Eckle, H.-G. Anfang, and R. J. Behm, "Reaction intermediates and side products in the methanation of CO and CO_2 over supported Ru catalysts in H_2-rich reformate gases," *Journal of Physical Chemistry C*, vol. 115, no. 4, pp. 1361–1367, 2011.

[29] I. Graça, L. V. González, M. C. Bacariza et al., "CO_2 hydrogenation into CH_4 on NiHNaUSY zeolites," *Applied Catalysis B: Environmental*, vol. 147, pp. 101–110, 2014.

[30] S. Tada, T. Shimizu, H. Kameyama, T. Haneda, and R. Kikuchi, "Ni/CeO_2 catalysts with high CO_2 methanation activity and high CH_4 selectivity at low temperatures," *International Journal of Hydrogen Energy*, vol. 37, no. 7, pp. 5527–5531, 2012.

[31] H. Takano, K. Izumiya, N. Kumagai, and K. Hashimoto, "The effect of heat treatment on the performance of the Ni/(Zr-Sm oxide) catalysts for carbon dioxide methanation," *Applied Surface Science*, vol. 257, no. 19, pp. 8171–8176, 2011.

[32] S. Hwang, J. Lee, U. G. Hong et al., "Methanation of carbon dioxide over mesoporous Ni–Fe–Ru–Al2O3 xerogel catalysts: effect of ruthenium content," *Journal of Industrial and Engineering Chemistry*, vol. 19, no. 2, pp. 698–703, 2013.

[33] E. Jwa, S. B. Lee, H. W. Lee, and Y. S. Mok, "Plasma-assisted catalytic methanation of CO and CO_2 over Ni–zeolite catalysts," *Fuel Processing Technology*, vol. 108, pp. 89–93, 2013.

[34] H. Liu, X. Zou, X. Wang, X. Lu, and W. Ding, "Effect of CeO_2 addition on Ni/Al_2O_3 catalysts for methanation of carbon dioxide with hydrogen," *Journal of Natural Gas Chemistry*, vol. 21, no. 6, pp. 703–707, 2012.

[35] J. Liu, W. Bing, X. Xue et al., "Alkaline-assisted Ni nanocatalysts with largely enhanced low-temperature activity toward CO_2 methanation," *Catalysis Science and Technology*, vol. 6, no. 11, pp. 3976–3983, 2016.

[36] A. Trovarelli, C. Deleitenburg, G. Dolcetti, and J. L. Lorca, "CO_2 methanation under transient and steady-state conditions over Rh/CeO_2 and CeO_2-promoted Rh/SiO_2: the role of surface and bulk ceria," *Journal of Catalysis*, vol. 151, no. 1, pp. 111–124, 1995.

[37] A. Trovarelli, C. De Leitenburg, and G. Dolcetti, "CO and CO_2 hydrogenation under transient conditions over $Rh–CeO_2$: novel positive effects of metal–support interaction on catalytic activity and selectivity," *Journal of the Chemical Society, Chemical Communications*, no. 7, pp. 472–473, 1991.

[38] J. M. Rynkowski, T. Paryjczak, A. Lewicki, M. I. Szynkowska, T. P. Maniecki, and W. K. Jóźwiak, "Characterization of Ru/CeO_2-Al_2O_3 catalysts and their performance in CO_2 methanation," *Reaction Kinetics and Catalysis Letters*, vol. 71, no. 1, pp. 55–64, 2000.

[39] F. Ocampo, B. Louis, L. Kiwi-Minsker, and A.-C. Roger, "Effect of Ce/Zr composition and noble metal promotion on nickel based $Ce_xZr_{1-x}O_2$ catalysts for carbon dioxide methanation," *Applied Catalysis A: General*, vol. 392, no. 1-2, pp. 36–44, 2011.

[40] P. A. U. Aldana, F. Ocampo, K. Kobl et al., "Catalytic CO_2 valorization into CH_4 on Ni-based ceria-zirconia. Reaction mechanism by operando IR spectroscopy," *Catalysis Today*, vol. 215, pp. 201–207, 2013.

[41] F. Ocampo, B. Louis, and A. Roger, "Methanation of carbon dioxide over nickel-based $Ce_{0.72}Zr_{0.28}O2$ mixed oxide catalysts prepared by sol–gel method," *Applied Catalysis A: General*, vol. 369, no. 1-2, pp. 90–96, 2009.

[42] H. C. Yao and Y. F. Y. Yao, "Ceria in automotive exhaust catalysts: I. Oxygen storage," *Journal of Catalysis*, vol. 86, no. 2, pp. 254–265, 1984.

[43] W. Wei and G. Jinlong, "Methanation of carbon dioxide: an overview," *Frontiers of Chemical Science and Engineering*, vol. 5, no. 1, pp. 2–10, 2011.

[44] L. Xu, H. Zhao, H. Song, and L. Chou, "Ordered mesoporous alumina supported nickel based catalysts for carbon dioxide reforming of methane," *International Journal of Hydrogen Energy*, vol. 37, no. 9, pp. 7497–7511, 2012.

[45] J. Zhang, Z. Xin, X. Meng, and M. Tao, "Synthesis, characterization and properties of anti-sintering nickel incorporated MCM-41 methanation catalysts," *Fuel*, vol. 109, pp. 693–701, 2013.

[46] G. Du, S. Lim, Y. Yang, C. Wang, L. Pfefferle, and G. L. Haller, "Methanation of carbon dioxide on Ni-incorporated MCM-41 catalysts: the influence of catalyst pretreatment and study of steady-state reaction," *Journal of Catalysis*, vol. 249, no. 2, pp. 370–379, 2007.

[47] D. P. Vargas, L. Giraldo, and J. C. Moreno-Piraján, "CO_2 adsorption on activated carbon honeycomb-monoliths: a comparison of langmuir and tóth models," *International Journal of Molecular Sciences*, vol. 13, no. 12, pp. 8388–8397, 2012.

[48] A. Samanta, A. Zhao, G. K. H. Shimizu, P. Sarkar, and R. Gupta, "Post-combustion CO_2 capture using solid sorbents: a review," *Industrial & Engineering Chemistry Research*, vol. 51, no. 4, pp. 1438–1463, 2012.

[49] N. P. Wickramaratne and M. Jaroniec, "Activated carbon spheres for CO_2 adsorption," *ACS Applied Materials and Interfaces*, vol. 5, no. 5, pp. 1849–1855, 2013.

[50] K. Li, S. Tian, J. Jiang, J. Wang, X. Chen, and F. Yan, "Pine cone shell-based activated carbon used for CO_2 adsorption," *Journal of Materials Chemistry A*, vol. 4, no. 14, pp. 5223–5234, 2016.

[51] N. N. Ha, N. T. T. Ha, L. Van Khu, and L. M. Cam, "Theoretical study of carbon dioxide activation by metals (Co, Cu, Ni) supported on activated carbon," *Journal of Molecular Modeling*, vol. 21, no. 12, article 322, 2015.

[52] P. T. M. Pham, M. T. Le, T. T. Nguyen, E. Bruneel, and I. Van Driessche, "The influence of deposition methods of support layer on cordierite substrate on the characteristics of a $MnO_2–NiO–Co_3O_4/Ce_{0.2}Zr_{0.8}O_2$/cordierite three way catalyst," *Materials*, vol. 7, no. 9, pp. 6237–6253, 2014.

[53] C. E. Hori, H. Permana, K. Y. S. Ng et al., "Thermal stability of oxygen storage properties in a mixed CeO_2-ZrO_2 system," *Applied Catalysis B: Environmental*, vol. 16, no. 2, pp. 105–117, 1998.

[54] P. Duwez and F. Odell, "Phase relationships in the system zirconia—ceria," *Journal of the American Ceramic Society*, vol. 33, no. 9, pp. 274–283, 1950.

[55] Q. Huang, X. Xue, and R. Zhou, "Influence of interaction between CeO2 and USY on the catalytic performance of CeO2–USY catalysts for deep oxidation of 1,2-dichloroethane," *Journal of Molecular Catalysis A: Chemical*, vol. 331, no. 1-2, pp. 130–136, 2010.

[56] E. Sahle-Demessie, V. G. Devulapelli, and A. A. Hassan, "Hydrogenation of anthracene in supercritical carbon dioxide solvent using Ni supported on Hβ-Zeolite catalyst," *Catalysts*, vol. 2, no. 1, pp. 85–100, 2012.

[57] S. Xu and X. Wang, "Highly active and coking resistant $Ni/CeO_2–ZrO_2$ catalyst for partial oxidation of methane," *Fuel*, vol. 84, no. 5, pp. 563–567, 2005.

[58] F. Cova, D. G. A. Pintos, A. Juan, and B. Irigoyen, "A first-principles modeling of Ni interactions on $CeO_2–ZrO_2$ mixed oxide solid solutions," *The Journal of Physical Chemistry C*, vol. 115, pp. 7456–7465, 2011.